Adjusting the DNA Interaction and Anticancer Activity of Pt(II) N-Heterocyclic Carbene Complexes by Steric Shielding of the Trans Leaving Group

Muenzner, Julienne K.; Rehm, Tobias; Biersack, Bernhard; Casini, Angela; de Graaf, Inge A. M.; Worawutputtapong, Pawida; Noor, Awal; Kempe, Rhett; Brabec, Viktor; Kasparkova, Jana

Published in:
Journal of Medicinal Chemistry

DOI:
10.1021/acs.jmedchem.5b00896

Journal of Medicinal Chemistry

Article

pubs.acs.org/jmc

Adjusting the DNA Interaction and Anticancer Activity of Pt(II) N-Heterocyclic Carbene Complexes by Steric Shielding of the Trans Leaving Group

Julienne K. Muenzner,[†] Tobias Rehm,[†] Bernhard Biersack,[†] Angela Casini,[‡] Inge A. M. de Graaf,[‡] Pawida Worawutputtapong,[‡] Awal Noor,[§] Rhett Kempe,[§] Viktor Brabec,[∥] Jana Kasparkova,[⊥] and Rainer Schobert*[,†]

[†]Organic Chemistry Laboratory, [§]Lehrstuhl fuer Anorganische Chemie II (Catalyst Design), University Bayreuth, Universitaetsstrasse 30, 95440 Bayreuth, Germany

[‡]Department of Pharmacokinetics, Toxicology and Targeting, Research Institute of Pharmacy, University of Groningen, Antonius Deusinglaan 1, 9713 AV Groningen, The Netherlands

[∥]Institute of Biophysics, Academy of Sciences of the Czech Republic, CZ-61265 Brno, Czech Republic

[⊥]Department of Biophysics, Faculty of Science, Palacky University, 17. listopadu 12, CZ-77146 Olomouc, Czech Republic

Supporting Information

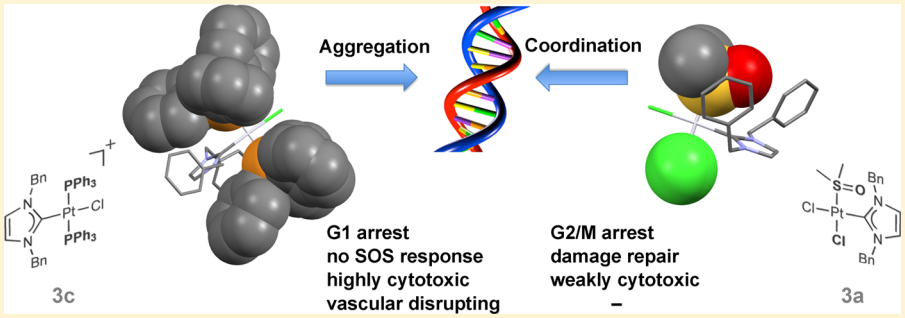

ABSTRACT: Five platinum(II) complexes bearing a (1,3-dibenzyl)imidazol-2-ylidene ligand but different leaving groups trans to it were examined for cytotoxicity, DNA and cell cycle interference, vascular disrupting properties, and nephrotoxicity. The cytotoxicity of complexes **3a**–**c** increased with the steric shielding of their leaving chloride ligand, and complex **3c**, featuring two triphenylphosphanes, was the most efficacious, with submicromolar IC_{50} concentrations. Complexes **3a**–**c** interacted with DNA in electrophoretic mobility shift and ethidium bromide binding assays. The cationic complex **3c** did not bind coordinatively to DNA but led to its aggregation, damage that is not amenable to the usual repair mechanisms. Accordingly, it arrested the cell cycle of melanoma cells in G1 phase, whereas *cis*-dichlorido[(1,3-dibenzyl)imidazol-2-ylidene](dimethyl sulfoxide) platinum(II) **3a** induced G2/M phase arrest. Complex **3c** also disrupted the blood vessels in the chorioallantoic membrane of fertilized chicken eggs. *Ex vivo* studies using precision-cut tissue slices suggested the nephrotoxicities of **3a**–**c** to be clinically manageable.

INTRODUCTION

Since the discovery of its antitumor activity in the late 1960s by Rosenberg et al.,[1] cisplatin has become one of the leading drugs in cancer chemotherapy. Only two additional platinum(II) drugs, carboplatin and oxaliplatin, have been approved in the US and EU for the treatment of certain forms of cancer.[2−4] These complexes are known to interact with DNA as their main cellular target and to form DNA adducts by coordination of the *cis*-$[Pt(R\text{-}NH_2)_2]$ fragment to the N-7 atom of purine bases, preferentially guanine.[2,4] The formation of intra- or interstrand cross-links leads to an impairment of DNA replication and transcription, G2/M phase cell cycle arrest, and, eventually, cancer cell apoptosis. However, the clinical application of platinum drugs is associated with unwanted side effects such as nephrotoxicity, ototoxicity, and neurotoxicity.[4−6] Resistance, both inherent and acquired, is another common problem.[3,4] A host of further platinum complexes was synthesized with the intention of overcoming or at least ameliorating the negative aspects of platinum chemotherapy, among them are compounds with trans coordination at the platinum center, complexes of platinum(IV), and heteronuclear complexes. In recent years, antitumoral complexes of other transition metals, including gold, silver, palladium, copper, rhodium, and ruthenium, bearing N-heterocyclic carbene (NHC) ligands have come to the fore.[7−11] This is, in part, owed to the stability of these Wanzlick-type carbenes and to the possibility of varying their substituents for pharmacological optimization. Various modes of action were

Received: June 10, 2015
Published: July 16, 2015

DOI: 10.1021/acs.jmedchem.5b00896
J. Med. Chem. 2015, 58, 6283−6292

identified such as interference with cell cycle progression, mitochondrial function, or DNA repair.[7−13] DNA is not necessarily a target any more, not even for platinum(II) complexes.[14,15] Herein, we report five new Pt(II) NHC complexes, their crystal structures, the dependency of their DNA interactions and anticancer/antivascular properties on the nature and position of their ligands, and their nephrotoxicities in an *ex vivo* rat model.

RESULTS AND DISCUSSION

Complex Syntheses and Structures. On the basis of protocols by Newman et al.,[16] we prepared five new [(1,3-dibenzyl)imidazol-2-yl]platinum(II) carbene complexes (Scheme 1). The known silver carbene complex **1**[17,18] was

Scheme 1. Synthesis of Platinum(II) NHC Complexes 2 and 3a−d[a]

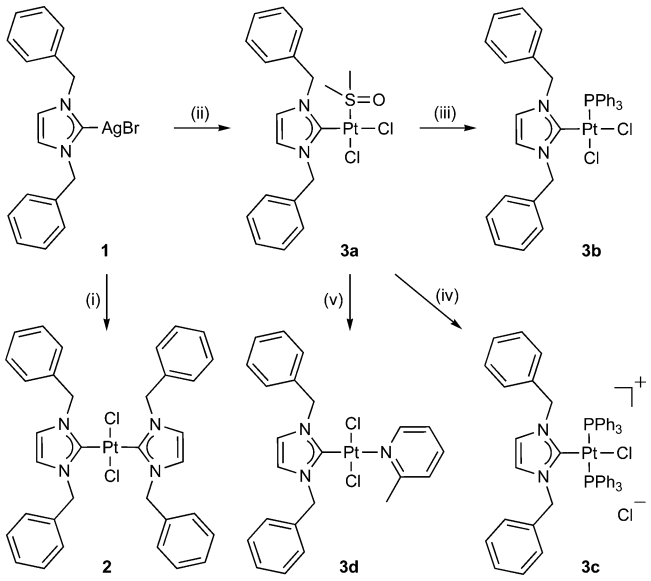

[a]Reagents and conditions: (i) 0.5 equiv K_2PtCl_4, CH_2Cl_2, rt, 24 h; (ii) K_2PtCl_4, DMSO, 60 °C, 24 h; (iii) 1 equiv PPh_3, CH_2Cl_2, rt, 1.5 h; (iv) 5 equiv PPh_3, CH_2Cl_2, rt, 30 min; (v) 2-picoline, CH_2Cl_2, rt, 6 days.

reacted with one-half an equivalent of K_2PtCl_4 in dichloromethane to give *trans*-$(NHC)_2PtCl_2$ complex **2**. The completion of this transmetalation was monitored by the upfield shift of the ^{13}C NMR signal of the carbene C atom from 181.3 ppm in complex **1** to 166.0 ppm in complex **2**. *cis*-(NHC)(DMSO)$PtCl_2$ complex **3a** was obtained from reaction of complex **1** with one equivalent of K_2PtCl_4 in DMSO at 60 °C. Its ^1H NMR spectrum showed equivalent imidazole and DMSO signals, whereas the benzyl protons were inequivalent and split into two doublets, 0.06 ppm apart and coupling with $^2J_{AB}$ = 15 Hz. This confirms the cis configuration of NHC and DMSO ligands as well as a perpendicular orientation of the imidazole ring relative to the plane spanned by the $PtCl_2$(DMSO) fragment (Figure 1). The ^{13}C NMR resonance of the carbene C atom of **3a** lay at 144.9 ppm, and the ^{195}Pt spectrum showed a signal at 962 ppm. The DMSO ligand of **3a** was readily replaced upon reaction with one equivalent of triphenylphosphane in dichloromethane at room temperature to afford *cis*-(NHC)$(PPh_3)PtCl_2$ complex **3b**, which was precipitated by addition of *n*-hexane. Its ^1H NMR spectrum showed the benzylic protons as two doublets, 1.32 ppm apart and coupling with $^2J_{AB}$ = 14 Hz. The ^{13}C NMR signal of the carbene C atom appeared as a doublet at 149.9 ppm with $^2J_{CP}$ = 8.1 Hz; the ^{195}Pt spectrum revealed a doublet at 504 ppm with $^1J_{PtP}$ = 3915 Hz. This $^{31}P-^{195}Pt$ coupling was also visible in the ^{31}P NMR for the signal at 8.49 ppm with $^1J_{PPt}$ = 3894 Hz. The ionic bis(triphenylphosphane) complex **3c** was obtained by adding a 5-fold excess of PPh_3 to the DMSO precursor **3a** in dichloromethane. After 30 min at room temperature, *n*-hexane was added to precipitate the pure product complex **3c**. Extended reaction periods (>5 h) led to formation of *cis*-dichloridobis(triphenylphosphane)platinum(II).

The benzylic protons gave rise to a singlet in the ^1H NMR spectrum of **3c**, which proves that the two phosphane ligands stand trans to each other. Their presence is also indicated by triplets in the ^{13}C NMR spectrum for the carbene C atom at 145.0 ppm with $^2J_{CP}$ = 10 Hz and for the platinum in the ^{195}Pt NMR spectrum at 159.9 ppm with $^1J_{PtP}$ = 2503 Hz. The corresponding $^{31}P-^{195}Pt$ coupling in the ^{31}P NMR for the signal at 17.5 ppm was $^1J_{PPt}$ = 2503 Hz. Complex **3d** was obtained from reaction of **3a** with 2-picoline. Integrations and the singlet signal for the benzylic hydrogens in the ^1H NMR spectrum confirm **3d** to be the *trans*-(NHC)(2-picoline)$PtCl_2$ complex. Figure 1 depicts the benzylic proton signals in the ^1H NMR spectra of complexes **1** and **3a−c**.

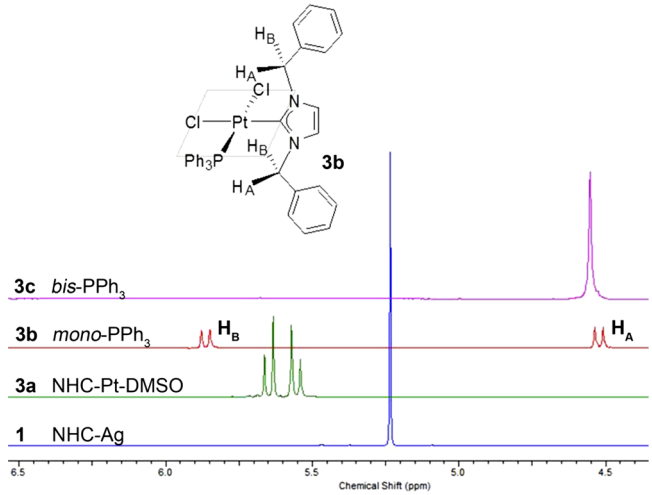

Figure 1. Benzylic proton signals in ^1H NMR spectra of complexes **1** and **3a−c**.

Crystals suitable for X-ray diffraction analyses were grown by slow infusion of hexane into saturated solutions of **3a** or **3b** in dichloromethane and **3c** in chloroform kept at 0 °C. Figure 2 shows the molecular structures. The characteristic bond lengths and angles were quite similar for all three complexes. The distances between the metal and the carbene carbon atoms C1 were in the range of 1.95−1.97 Å, and those between the metal and the leaving chloride Cl1 were about 2.35 Å. The C1−Pt−Cl1 angles were in the range of 174° (**3b**) to 177° (**3a**, **3c**). However, the potential leaving chloride Cl1 gets distinctly more shielded when going from **3a** to **3b** to **3c**.

Biological Evaluation: Cancer Cell Growth Inhibition. Complexes **2** and **3a−d** were screened for antiproliferative activity against a panel of seven cancer cell lines using the MTT assay.[19] All compounds showed dose-dependent inhibition of cell growth, with IC_{50} values mainly in the low micromolar range even against cisplatin-resistant cell lines such as HT-29 colon carcinoma.[20,21] Table 1 summarizes the IC_{50} values calculated

DOI: 10.1021/acs.jmedchem.5b00896
J. Med. Chem. 2015, 58, 6283−6292

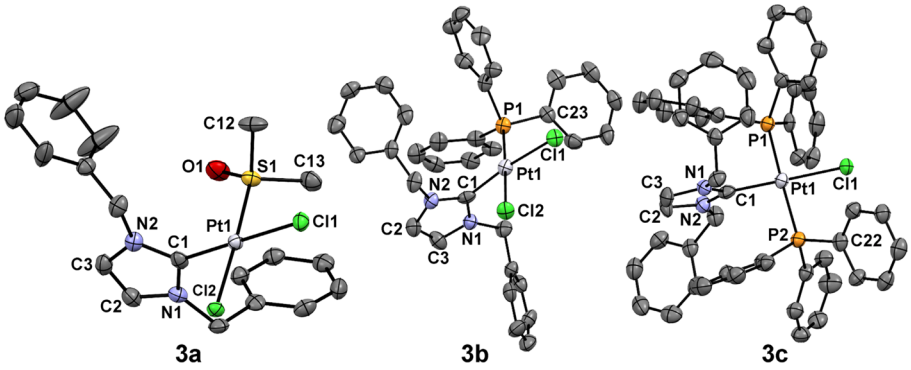

Figure 2. Molecular structures of chloridoplatinum(II) carbene complexes **3a**–**c** (cation only) as thermal ellipsoid representations at 50% probability level showing the atomic numbering schemes (H atoms omitted). Selected bond lengths [Å] and angles [deg]: **3a**: Pt1–C1 1.972(8), Pt1–Cl1 2.357(2), Pt1–Cl2 2.339(2), Pt1–S1 2.205(2), C1–N1 1.35(1), C1–N2 1.34(1), C2–N1 1.36(1), C3–N2 1.38(1), C1–Pt1–Cl1 177.6(2), S1–Pt1–Cl2 177.58(6), C1–Pt1–S1 90.3(2); **3b**: Pt1–C1 1.95(1), Pt1–Cl1 2.349(3), Pt1–Cl2 2.360(3), Pt1–P1 2.236(3), C1–N1 1.35(1), C1–N2 1.37(1), C2–N2 1.39(1), C3–N1 1.39(1), P1–C23 1.81(1), C1–Pt1–Cl1 173.5(3), P1–Pt1–Cl2 178.0(1), C1–Pt1–P1 94.0(3); **3c**: Pt1–C1 1.975(6), Pt1–Cl1 2.350(1), Pt1–P1 2.326(1), Pt1–P2 2.324(2), C1–N1 1.35(1), C1–N2 1.358(8), C2–N2 1.377(9), C3–N1 1.388(7), P2–C22 1.808(7), C1–Pt1–Cl1 177.3(2), P1–Pt1–P2 174.06(6), C1–Pt1–P1 87.59(6), C1–Pt1–P2 89.90(6).

Table 1. Inhibitory Concentrations[a] IC_{50} [μM] of Cisplatin and Complexes 2 and 3a–d when Applied to Human Cancer Cell Lines and Fibroblasts

compound/cell line	2	3a	3b	3c	3d	cisplatin
518A2	12.0 ± 0.3	27.7 ± 1.2	7.5 ± 0.4	0.32 ± 0.02	11.4 ± 0.5	5.3 ± 0.4
Panc-1	20.4 ± 1.3	20.6 ± 0.3	7.7 ± 0.5	0.32 ± 0.01	5.1 ± 0.3	4.8 ± 0.7
MCF-7/Topo	7.7 ± 0.7	31.2 ± 1.2	3.9 ± 0.3	0.15 ± 0.01	5.1 ± 0.2	10.6 ± 0.7
KB-V1/Vbl	>50	>50	4.5 ± 0.5	2.1 ± 0.2	8.6 ± 1.4	>100
HCT-116	11.3 ± 0.7	18.0 ± 1.4	6.7 ± 0.4	0.28 ± 0.06	5.9 ± 1.1	5.0 ± 0.6
HT-29	8.4 ± 0.3	22.7 ± 0.7	9.6 ± 0.4	0.85 ± 0.05	42.2 ± 4.8	>100
DLD-1	14.7 ± 3.4	27.0 ± 1.6	2.5 ± 0.4	0.92 ± 0.09	32.3 ± 3.4	32.6 ± 2.4
CCD18Co	35.8 ± 11.4	>50	14.5 ± 2.1	2.8 ± 0.1	>50	>100

[a]Values derived from dose–response curves obtained by measuring the percentage of viable cells relative to that of untreated controls after 72 h of incubation using the MTT assay; human cancer cell lines: 518A2 melanoma, Panc-1 pancreatic ductular adenocarcinoma, MCF-7/Topo breast adenocarcinoma, KB-V1/Vbl cervix carcinoma, HCT-116 and HT-29 colon carcinoma, and DLD-1 colorectal adenocarcinoma; nonmalignant cell line: CCD18Co human colon fibroblasts. Values represent means of four experiments ± SD.

from dose–response curves. The antiproliferative effects were dependent on the nature and configuration of the auxiliary non-NHC ligands. Biscarbene complex **2** was active, with low-double-digit micromolar IC_{50} values across the panel. *cis*-Dichlorido(monophosphane) complex **3b** and *trans*-dichlorido(2-picoline) complex **3d** were of similar efficacy against the cisplatin-sensitive cancer cell lines, with single-digit IC_{50} figures. While complex **3b** was also efficacious against the cisplatin-resistant HT-29 and DLD-1 colon carcinoma cells, complex **3d** was virtually inactive against these cell lines. *cis*-Dichlorido(DMSO) complex **3a** was least active, on average. Strikingly, *trans*-bisphosphane complex **3c** reached nanomolar IC_{50} values against all but one cancer cell line. In principle, this could be due to its ionic nature enabling its cellular uptake via cation transporters that are frequently overexpressed in cancer cells.[22−26] However, when we measured the lipophilicities (i.e., log P values) and the platinum content of treated HCT-116 colon carcinoma cells, we found that both increased like the cytotoxicities when going from **3a** to **3b** to **3c** (cf. Supporting Information, Table S2), presumably because of the large organic PPh_3 groups.

DNA Interaction. Complexes **2** and **3a**–**d** were incubated with circular pBR322 plasmid DNA, and the resulting changes in the electrophoretic mobility of the plasmids' topological forms were monitored (Figure 3). The observed band shifts did not correlate with the cytotoxicities of the complexes. Complexes **2** and **3d**, both featuring a poor leaving ligand trans to the NHC ligand, did not alter the electrophoretic mobility of the DNA. In contrast, complexes **3a**–**c**, all featuring the good leaving ligand

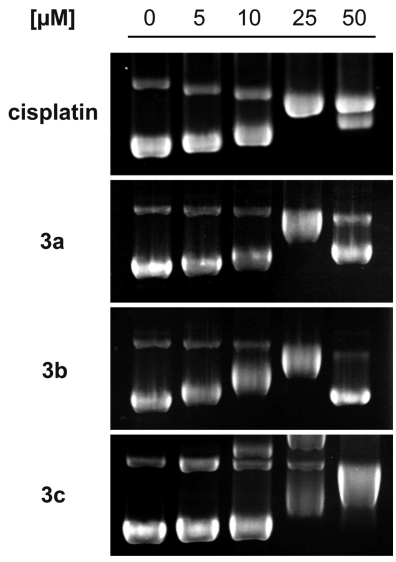

Figure 3. Interaction of cisplatin and complexes **3a**–**c** with circular pBR322 plasmid DNA, as observed by electrophoretic mobility shift assays (EMSA), after 24 h of incubation. Pictures are representative of at least two independent experiments.

DOI: 10.1021/acs.jmedchem.5b00896
J. Med. Chem. 2015, 58, 6283−6292

Cl, induced a concentration-dependent band shift. At higher complex concentrations (25 and 50 μM), a rewinding of the plasmid DNA occurred with renewed increase of the electrophoretic mobility. For the most cytotoxic complex **3c**, additional bands with even less electrophoretic mobility than that of the plasmid's open-circular (oc) form appeared for concentrations $\geq$10 μM. When 25 or 50 μM **3c** was applied, large amounts of plasmid DNA remained in the wells of the gel, suggesting that bigger DNA adducts had formed that cannot penetrate the pores of the agarose gel (for a full picture of EMSA gel with complex **3c**, cf. Supporting Information, Figure S1). Cisplatin accelerated the mobility of the relaxed form due to its bifunctional binding to DNA, which shortens and condenses the DNA helix.[27,28] In contrast, complexes **3a**–**c** accelerated the mobility of the relaxed form only marginally, indicating that they interact with DNA in a way fundamentally different from that of cisplatin.

In a fluorescence-based staining assay,[29,30] high-molecular-mass salmon sperm DNA (SS DNA) was incubated with cisplatin or complexes **3a**–**c** and was then stained with ethidium bromide (EtdBr), and the fluorescence of EtdBr–DNA adducts was measured (Figure 4). While complexes **3a** and **3b** reduced the

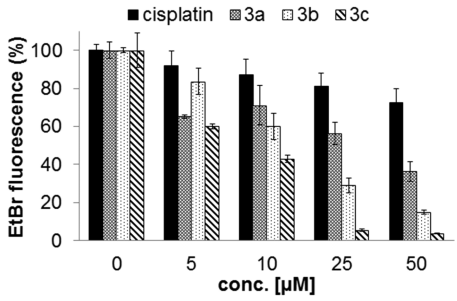

Figure 4. Relative ethidium bromide–DNA adduct fluorescence after preincubation with vehicle (set to 100%), cisplatin, or complexes **3a**–**c** (5, 10, 25, and 50 μM) for 2 h. Decreased fluorescence is indicative of inhibition of ethidium bromide intercalation into DNA.

EtdBr fluorescence to 36 and 15%, respectively, complex **3c** at the highest concentration prevented the intercalation of the fluorescent dye, leaving a residual fluorescence of only 4%.

In order to decide whether the effects observed in the EMSA and EtdBr staining studies originated from different amounts of Pt coordinatively bound to DNA or from an altogether different binding mode, more experiments were performed. Solutions of double-helical high-molecular-mass calf thymus (CT) DNA were incubated with compounds **3a**–**c** at an r_i of 0.05 in $NaClO_4$ (10 mM) at 37 °C (r_i is defined as the molar ratio of free platinum complex to nucleotide phosphates at the onset of incubation with DNA). At regular time intervals, aliquots of the reaction mixture were withdrawn, dialyzed against 1 M NaCl to remove all unbound platinum complex along with platinum complex fragments noncoordinatively bound to DNA, and assayed by flame atomic absorption spectrometry (FAAS) for platinum irreversibly (coordinatively) bound to DNA. Its amount increased with time (Figure 5A). $T_{50\%}$, the time by which half of the maximum amount of Pt was bound, was ca. 0.5 and 5.2 h for complexes **3a** and **3b**, respectively. Compound **3c** bound to DNA markedly slower. Essentially the same binding rates were observed in experiments with compounds **3a**–**c** at r_i = 0.1 (not shown). In addition, DNA was incubated with **3a**–**c** or cisplatin for 24 h, and then the samples were centrifuged through a Sephadex G50 column to remove free or noncovalently bound

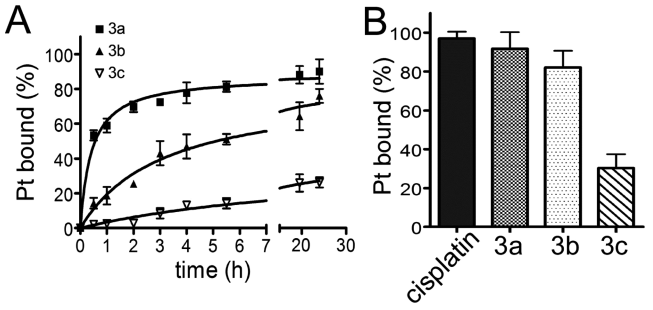

Figure 5. (A) Kinetics of the reaction of **3a**–**c** with double-helical CT DNA at r_i = 0.05 in $NaClO_4$ (10 mM) at 37 °C. Data represent mean ± SD values from three independent experiments. (B) The relative amount of Pt bound to DNA after 24 h of incubation with **3a**–**c** or cisplatin at 37 °C. Data represent mean ± SD values.

platinum and assayed by FAAS. Figure 5B shows that the ability of complexes **3a**–**c** to bind coordinatively to DNA decreased with increasing numbers of PPh_3 ligands, which might sterically restrict the contact with DNA or the hydrolysis of the leaving chloride. The upshot is that the amount of fragments of **3a**–**c** coordinatively bound to DNA correlates inversely with the cytotoxicity of these complexes against tumor cells.

These results, together with those of the EMSA and EtdBr studies, support the hypothesis that **3c** might interact with DNA predominantly via noncovalent interactions, facilitated by its positive charge. A similar behavior had already been described for compounds that effectively condense or aggregate DNA.[31−33] Moreover, when the blockage of EtdBr intercalation into CT DNA was assessed, the formation of aggregated DNA fibers in the solution was observed, especially at higher concentrations of compound **3c** (25 and 50 μM) and, to a lesser extent, also of compound **3b**. Therefore, the ability of complexes **3a**–**c** to initiate the condensation or aggregation of DNA was assessed by a light scattering assay[34] that measures the intensity of light scattered by a diluted DNA solution at a 90° angle with respect to the incident beam. This intensity increases in a concentration-dependent manner in the presence of condensing agents due to the formation of condensed DNA particles. The EC_{50} value represents the concentration of the test compound at which 50% of the total amount of DNA is condensed (Figure 6A). In keeping with the EMSA data, complex **3c** was the most efficient inducer of DNA aggregation, with an EC_{50} value of 0.51 ± 0.04 μM, whereas complex **3b** exhibited an EC_{50} value of 1.00 ± 0.02 μM, and complex **3a** failed to induce DNA condensation. The turbidity of the solutions was also determined UV/vis spectrophotometrically by monitoring the absorbance of CT

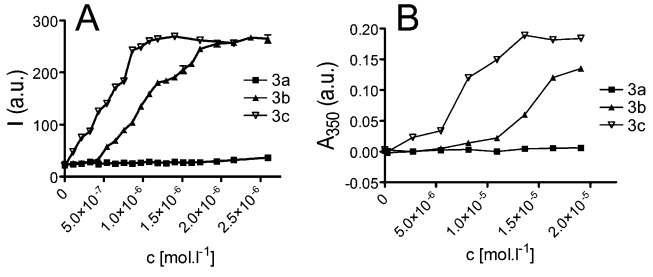

Figure 6. (A) Intensity of light scattered by CT DNA (1.5×10^{-6} M; 10 mM cacodylate, pH 7.2, 25 °C) in the presence various concentrations of **3a**–**c**. (B) Absorption of CT DNA (1×10^{-4} M; 10 mM NaCl, 10 mM TrisCl, pH 7.4, 25 °C) in the presence of **3a**–**c** at 350 nm.

DOI: 10.1021/acs.jmedchem.5b00896
J. Med. Chem. 2015, 58, 6283−6292

DNA at 350 nm (Figure 6B), which rose upon addition of **3b** or **3c**, indicating the onset of the condensation process,[35] and which kept increasing with growing concentration. Once more, complex **3a** did not lead to turbidity changes up to concentrations of ca. 20 μM.

Considering these results, the observed decrease of EtdBr fluorescence induced by complexes **3b** and **3c** (Figure 4) is likely the consequence of a reduced concentration of DNA amenable to EtdBr intercalation. The data indicate that the cytotoxicity against cancer cells of **3a**−**c** correlates with their ability to condense/aggregate DNA rather than with their ability to coordinatively bind to DNA. Taken together, the DNA interactions of (NHC)Pt(II) complexes bearing one or two triphenylphosphane ligands are significantly different from those of cisplatin. This was further corroborated by their effects on the morphology of growing *Escherichia coli*. Unlike cisplatin, complexes **3b** and **3c** did not induce filamentation and growth of the bacteria to a size 15 times longer than normal.[36,37] However, complex **3a** induced filamentous growth of some of the bacteria, albeit to a lesser extent than that with cisplatin (cf. Supporting Information, Figure S2). A final experiment demonstrating the peculiar DNA interaction of complexes **3a**−**c** as opposed to that of cisplatin was their failure to induce lysis in *E. coli* infected with bacteriophage λ,[38] which also proves that DNA damage caused by these complexes does not elicit the usual SOS repair machinery (cf. Supporting Information, Figure S3).

Cell Cycle Interference. The influence of the complexes **3a**−**c** on the cell cycle progression of 518A2 melanoma cells was analyzed using propidium iodide staining and flow cytometry (Figure 7). Cisplatin was used as a reference since a G2/M phase

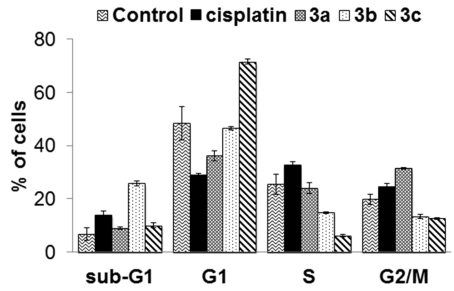

Figure 7. Effects of cisplatin and complexes **3a**−**c** on the cell cycle progression of 518A2 melanoma cells. Shown are the percentages of cells in G1, S, and G2/M phases and apoptotic cells (sub-G1), as obtained by flow cytometry after DNA staining with propidium iodide. Cells were treated with 50 μM cisplatin, 30 μM **3a**, 5 μM **3b**, or 500 nM **3c** for 24 h. Values represent means ± SD of three experiments.

arrest has already been reported as an essential step in its mechanism of action.[2,4,39,40] When 518A2 melanoma cells were treated with 50 μM of cisplatin for 24 h, a moderate accumulation of cells in the G2/M and S phases of the cell cycle as well as an increase of apoptotic cells was observed. Complex **3a** also arrested 518A2 cells in the G2/M phase of the cell cycle; however, it did so to a greater extent than cisplatin. Both cisplatin and complex **3a** reduced the number of cells in the G1 phase of the cell cycle. In contrast, complex **3b** did not induce any kind of cell cycle arrest but directly led to cell death at a concentration as low as 5 μM. Complex **3c** showed a completely different effect, namely, a marked accumulation of 518A2 cells in the G1 phase and a decrease of cells in the S phase. This is in line with the particular mode of interaction of **3c** with DNA, which probably prevents 518A2 melanoma cells from proceeding to S phase due to an impairment of DNA transcription and replication.

Vascular Disrupting Properties. Since we had found certain metal NHC complexes to be vascular disrupting,[10,11] we analyzed the effects of complexes **3a**−**c** on developing blood vessels in the chorioallantoic membrane (CAM) of fertilized chicken eggs as an *in vivo* model.[11,41,42] While complex **3b** showed only moderate vascular disrupting effects after 24 h, complexes **3a** and **3c** were highly effective as early as 6 h post treatment, disrupting the capillary reticulation and degrading even big blood vessels. Complex **3c** was the most effective compound and led to a complete destruction of blood vessels in the treated area of the CAM after 24 h. Cisplatin displayed a negligible effect on the developing vasculature, although it penetrated into the CAM rather deeply (Figure 8).

Nephrotoxicity. The organ toxicity of complexes **3a**−**c** in comparison to the nephrotoxic[5,6] cisplatin was studied using precision-cut tissue slices (PCTS) of rat kidneys that can be cultured *ex vivo* (Figure 9).[43,44] These slices represent viable explants with all cell types in their natural environment, thereby maintaining intercellular and cell−matrix interactions. They constitute a meaningful organ model that was previously applied for the toxicity assessment of cisplatin (kidney),[45] experimental gold compounds (liver, kidney, and colon),[46] and amino-ferrocenyl prodrugs (liver).[47]

Different concentrations of complexes **3a**−**c** were incubated with kidney slices (PCKS) for 24 h, and the tissue viability was determined by measuring the ATP content. Complexes **3a** and **3b** showed a moderate effect on the PCKS viability when compared to that with cisplatin, which reduced it to 50% at concentrations of ca. 10−15 μM. In contrast, complex **3c** was more toxic and reduced the PCKS viability to ∼30% at a concentration as low as 5 μM. It should be kept in mind, though, that complex **3c** was 15 times more efficacious than cisplatin against the cancer cell lines tested in the MTT assays and thus could possibly be administered to animals or patients at a correspondingly lower dosage.

The effects of different concentrations of complexes **3a** and **3c** on the histomorphology of PCKS were also assessed. The results confirm those of the ATP viability assay. Figure 10 shows representative pictures for the treatment with **3a**. The kidney slices were only slightly affected by 1 μM **3a**, although some toxic effects on tubular cells became apparent. More pronounced morphological alterations were observed upon treatment with 25 μM **3a**, whereas 100 μM of this compound led to outright kidney cell necrosis, indicated by the loss of nuclei. The strong impact of **3c** on the viability of PCKS shown in Figure 9 was mirrored by an induction of distinct cell necrosis in slices treated with concentrations as low as 1 μM (cf. Supporting Information, Figure S4).

■ CONCLUSIONS

This study showed that only NHC platinum(II) complexes with good leaving groups such as chloride trans to the NHC ligand, e.g., complexes **3a**−**c**, interact noticeably with DNA in electrophoretic mobility shift and ethidium bromide staining assays. However, this is not a prerequisite for high cytotoxicity against cancer cells, apparent from the efficacy of the nonbinders to DNA, complexes **2** and **3d**.

Within the series of *trans*-chlorido-[(1,3-dibenzyl)imidazol-2-ylidene]platinum(II) complexes **3a**−**c**, there is an increasing steric shielding of the leaving chloride by the two spectator ligands when going from **3a** (spectator ligands: chlorido and

DOI: 10.1021/acs.jmedchem.5b00896
J. Med. Chem. 2015, 58, 6283−6292

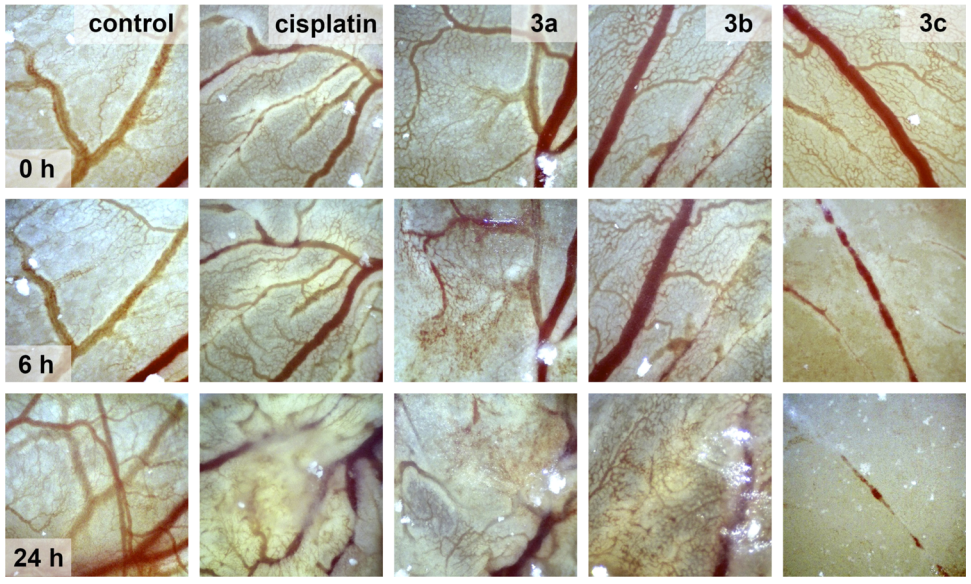

Figure 8. Effects of cisplatin and complexes **3a**–**c** when applied topically (10 nmol in 10 μL of H_2O) on developing vasculature in the chorioallantoic membrane of fertilized chicken eggs after 6 and 24 h of incubation. Control, respective amount of DMF (in a total volume of 10 μL of H_2O); images are representative of three independent experiments.

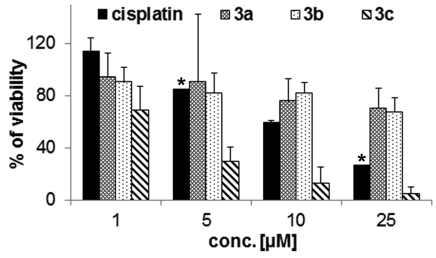

Figure 9. Viability of precision-cut kidney slices (PCKS) treated with different concentrations of cisplatin or complexes **3a**–**c** for 24 h, normalized by means of protein concentrations. The viability of control slices was set to 100%. Values represent means ± SD of at least two independent experiments performed in triplicate, except for starred bars, which were obtained from single experiments run in triplicate.

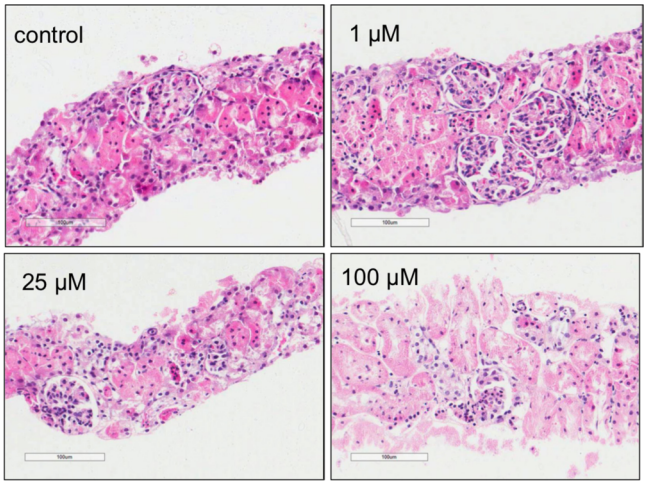

Figure 10. Morphology of PCKS treated with different concentrations of complex **3a** for 24 h; scale bars, 100 μm.

DMSO) to **3b** (chlorido and PPh_3) to **3c** (two PPh_3). Complex **3a** bound at the highest rate and to the greatest extent to double-helical CT DNA and resembled cisplatin most closely as to the pattern of the various DNA morphologies in the EMSA with circular pBR322 plasmid DNA. Like cisplatin, it led to a pronounced G2/M cell cycle arrest of 518A2 melanoma cells and to an SOS response in *E. coli* bacteria. In essence, complex **3a** most closely resembles cisplatin as to its effects on a cellular level and so is likely to bind to DNA also in a coordinating manner. Complex **3b** takes a middle position, resembling **3a** in terms of the effects in the EMSA yet differing in many other aspects. It bound less rapidly to CT DNA and in a way that generated light scattering adducts and turbidity in solution. It did not lead to G2/M cell cycle arrest in the melanoma cells but to an increased fraction of apoptotic cells, and it did not elicit an SOS response in *E. coli*. Complex **3c** binds to DNA predominantly by initiating its aggregation and precipitation to the effect of a G1 phase cell cycle arrest in the tested melanoma cells and a strong antiproliferative impact on all tested cancer cells avoiding the usual SOS response. It also showed a vascular disrupting effect, hitherto known only of NHC gold complexes. It remains to be shown whether a platinum center is altogether required or if effects similar to those of **3c** could also be induced by complexes of other central metals bearing sterically shielded leaving groups. Another issue to clarify in animal studies is whether the high organ toxicity of complexes that elicit DNA aggregation may be compensated by a reduction of the required dosage.

EXPERIMENTAL SECTION

Chemistry. *General.* Melting points are uncorrected; IR spectra were recorded on an FT-IR spectrophotometer with ATR sampling unit; NMR spectra were run on 300 and 500 MHz spectrometers; chemical shifts are given in ppm (δ) downfield from tetramethylsilane as internal standard, ^{195}Pt-NMR shifts are quoted relative to $\Xi(^{195}Pt)$ = 21.4 MHz; mass spectra: direct inlet, EI, 70 eV; HRMS: UPLC/Orbitrap MS system in ESI mode; microanalyses: Vario EL III elemental analyzer. The NHC ligand and its silver carbene complex **1** were prepared according to the literature.[17,18] All tested compounds were >95% pure by elemental analysis or UPLC/HRMS.

*trans-Dichlorido-bis(1,3-dibenzylimidazol-2-ylidene)platinum(II) (**2**).* A solution of 1,3-dibenzylimidazol-2-ylidene silver(I) bromide (50 mg, 0.115 mmol) in CH_2Cl_2 was treated with K_2PtCl_4 (23 mg, 0.057 mmol), and the resulting mixture was stirred at room temperature for 24

DOI: 10.1021/acs.jmedchem.5b00896
J. Med. Chem. 2015, 58, 6283–6292

h. The suspension was filtered, the filtrate was concentrated in vacuum, and the residue was recrystallized from CH_2Cl_2/hexane. Yield: 30 mg (0.039 mmol, 68%); off-white solid of mp 164−166 °C; ν_{max}/cm^{-1}: 3160, 3128, 3099, 3035, 2947, 1602, 1561, 1494, 1451, 1412, 1398, 1356, 1334, 1227, 1203, 1182, 1158, 1151, 1101, 1076, 1029, 960, 935, 918, 852, 825, 792, 770, 724, 704, 697, 662; ^{1}H NMR (300 MHz, $CDCl_3$) δ 5.27 (s, 8H), 6.8−6.9 (m, 4H), 7.3−7.4 (m, 20H); ^{13}C NMR (75.5 MHz, $CDCl_3$) δ 55.8, 121.5, 127.8, 128.7, 129.1, 135.3, 166.0; *m/z* (EI, %) 692 (3), 691 (4), 690 (4), 689 (2) [$M^+ - 2Cl$], 442 (2), 441 (2), 249 (10), 158 (23), 91 (100); HRMS: *m/z* calcd, 784.15496; found, 784.15338 [$C_{34}H_{32}PtN_4Cl_2Na^+$; $(M + Na)^+$].

*cis-Dichlorido-(1,3-dibenzylimidazol-2-ylidene)(dimethyl sufoxide)platinum(II) (**3a**).* A solution of 1,3-bis(benzyl)imidazol-2-ylidene silver(I) bromide (69 mg, 0.158 mmol) in DMSO was treated with K_2PtCl_4 (66 mg, 0.158 mmol), and the resulting mixture was stirred at 60 °C for 24 h. After adding CH_2Cl_2, the reaction mixture was filtered and the filtrate was washed with water and then dried over Na_2SO_4. The solvent was removed in vacuum, and the remainder ws recrystallized from CH_2Cl_2/hexane. Yield: 85 mg (0.143 mmol, 91%); colorless crystalline solid of mp 258 °C (dec.). Anal. Calcd for $C_{19}H_{22}Cl_2N_2OPtS$: C, 38.32; H, 4.23; N, 4.70. Found: C, 38.31; H, 3.91; N, 4.64. ν_{max}/cm^{-1}: 3091, 2933, 2836, 1611, 1585, 1511, 1455, 1441, 1350, 1303, 1245, 1175, 1111, 1028, 822, 773, 729, 702, 686, 658; ^{1}H NMR (500 MHz, $CDCl_3$) δ 3.16 (s, 6H), 5.70 (ABq, $\Delta\delta = 0.06$, $^2J_{AB} = 15$ Hz, 4H), 6.83 (s, 2H), 7.32−7.45 (m, 10H); ^{13}C NMR (125 MHz, $CDCl_3$) δ 45.5, 54.5, 121.4, 128.3, 128.6, 129.2, 135.1, 144.9; ^{195}Pt NMR ($CDCl_3$) δ 962 ppm; *m/z* (EI, %) 592 (15) [M^+], 556 (10) [$M^+ - Cl$], 521 (4) [$M^+ - Cl$], 441 (81), 349 (9), 247 (9), 157 (22), 91 (37), 78 (100), 63 (98); HRMS: *m/z* calcd, 556.07836; found, 556.07788 [$C_{19}H_{22}N_2OClPtS^+$; $(M - Cl)^+$]. Crystallographic data were deposited with The Cambridge Crystallographic Data Centre (CCDC) under no. 1062990.

*cis-Dichlorido-(1,3-dibenzylimidazol-2-ylidene)-(triphenylphosphane)platinum(II) (**3b**).* Triphenylphosphane (13 mg, 0.051 mmol) was slowly added to a solution of complex **3a** (30 mg, 0.051 mmol) in CH_2Cl_2, and the resulting mixture was stirred at room temperature for 90 min. The volatiles were removed in vacuum, and the remaining crude product was purified by recrystallization from CH_2Cl_2/hexane. Yield: 18 mg (0.023 mmol, 46%); colorless crystalline solid of mp 316 °C (dec.). Anal. Calcd for $C_{35}H_{31}Cl_2N_2PPt$: C, 54.13; H, 4.02; N, 3.61. Found: C, 53.52; H, 4.57; N, 3.47. ν_{max}/cm^{-1}: 3059, 3041, 1497, 1483, 1457, 1435, 1309, 1261, 1232, 1185, 1162, 1101, 1074, 1028, 999, 823, 726, 693, 617, 577; ^{1}H NMR (300 MHz, $CDCl_3$) δ 4.52 (d, $^2J_{AB}$ = 14.3 Hz, 2H), 5.84 (d, $^2J_{AB}$ = 14.3 Hz, 2H), 6.37 (s, 2H), 7.22−7.31 (m, 10H), 7.32−7.40 (m, 6H), 7.44−7.60 (m, 9H); ^{13}C NMR (75.5 MHz, $CDCl_3$) δ 54.3, 120.2, 128.4 (d, $^2J_{CP}$ = 11 Hz), 128.6, 128.8, 129.3, 129.5 (d, $^1J_{CP}$ = 63 Hz), 131.0 (d, $^3J_{CP}$ = 2.3 Hz), 134.1 (d, $^2J_{CP}$ = 11 Hz), 134.3, 149.9 (d, $^2J_{CP}$ = 8.1 Hz); ^{31}P NMR (121 MHz, $CDCl_3$) δ 8.49 ($^1J_{PPt}$ = 3894 Hz); ^{195}Pt NMR ($CDCl_3$) δ 504 ppm (d, $^1J_{PtP}$ = 3915 Hz); *m/z* (EI, %) 776 (6) [M^+], 740 (15) [$M^+ - Cl$], 703 (14) [$M^+ - 2Cl$], 689 (7), 456 (10), 442 (10), 337 (7), 297 (27), 262 (100), 247 (35), 183 (61), 91 (43); HRMS: *m/z* calcd, 740.15556; found, 740.15454 [$C_{35}H_{31}N_2ClPPt^+$; $(M - Cl)^+$]. Crystallographic data were deposited with The Cambridge Crystallographic Data Centre CCDC under no. 1062991.

*trans-Chlorido-(1,3-dibenzylimidazol-2-ylidene)bis-(triphenylphosphane)platinum(II) chloride (**3c**).* Triphenylphosphane (55 mg, 0.210 mmol) was slowly added to a solution of complex **3a** (25 mg, 0.042 mmol) in CH_2Cl_2, and the resulting mixture was stirred at room temperature for 30 min. The solvent was removed in vacuum, and the residue recrystallized from CH_2Cl_2/hexane. Yield: 23 mg (0.022 mmol, 53%); colorless crystalline solid of mp 117 °C. Anal. Calcd for $C_{53}H_{46}Cl_2N_2P_2Pt$: C, 61.27; H, 4.46; N, 2.70. Found: C, 59.54; H, 4.77; N, 2.74. ν_{max}/cm^{-1}: 3053, 2922, 2854, 1572, 1581, 1456, 1435, 1415, 1358, 1311, 1234, 1183, 1096, 1028, 999, 830, 744, 727, 689, 619; ^{1}H NMR (500 MHz, $CDCl_3$) δ 4.54 (s, 4H), 6.80 (d, $^3J_{HH}$ = 7.5 Hz, 4H), 6.94 (s, 2H), 6.98 (t, $^3J_{HH}$ = 7.5 Hz, 4H), 7.17 (t, $^3J_{HH}$ = 7.5 Hz, 2H), 7.28−7.68 (m, 30H); ^{13}C NMR (125 MHz, $CDCl_3$) δ 54.7, 122.9, 128.0 (t, $^1J_{CP}$ = 29 Hz), 128.5, 128.6, 128.7, 128.9, 129.2, 129.2 (t, $^3J_{CP}$ = 5.5 Hz), 129.5, 132.0, 132.3, 134.1, 145.0 (t, $^2J_{CP}$ = 10 Hz); ^{31}P NMR (202 MHz, $CDCl_3$) δ 17.5 ($^1J_{PPt}$ = 2503 Hz); ^{195}Pt NMR ($CDCl_3$) δ 159.9 ppm (t, $^1J_{PtP}$ = 2503 Hz); *m/z* (EI, %) 778 (6) [$M^+ - PPh_3$], 742 (10) [$M^+ - Cl - PPh_3$], 705 (10) [$M^+ - 2Cl - PPh_3$], 614 (2), 457 (7), 443 (6), 378 (5), 263 (100), 248 (25), 184 (45), 108 (21), 91 (27); HRMS: *m/z* calcd, 1002.24670; found, 1002.24280 [$C_{53}H_{46}N_2ClP_2Pt^+$; $(M - Cl)^+$]. Crystallographic data were deposited with The Cambridge Crystallographic Data Centre CCDC under no. 1062992.

*trans-Dichlorido-(1,3-dibenzylimidazol-2-ylidene)(2-picoline)-platinum(II) (**3d**).* 2-Picoline (100 μL, 1.01 mmol) was slowly added to a solution of complex **3a** (32 mg, 0.054 mmol) in CH_2Cl_2, and the resulting mixture was stirred at room temperature for 6 days. It was washed with water, the organic phase was dried over Na_2SO_4 and evaporated to leave a residue that was recrystallized from CH_2Cl_2/hexane. Yield: 18 mg (0.030 mmol, 55%); off-white solid of mp 226 °C (dec.); ν_{max}/cm^{-1}: 3166, 3055, 3030, 2836, 1610, 1571, 1489, 1455, 1421, 1349, 1294, 1226, 1208, 1157, 1112, 1030, 824, 764, 725, 702, 690, 595, 563; ^{1}H NMR (300 MHz, $CDCl_3$) δ 3.15 (s, 3H), 5.94 (s, 4H), 6.68 (s, 2H), 7.18−7.24 (m, 1H), 7.27 (d, $^3J_{HH}$ = 7.7 Hz, 1H), 7.32−7.44 (m, 6H), 7.51−7.59 (m, 4H), 7.63 (td, $^3J_{HH}$ = 7.7, 1.6 Hz, 1H), 8.85 (dt, $^3J_{HH}$ = 4.9, 0.8 Hz, 1H); ^{13}C NMR (75.5 MHz, $CDCl_3$) δ 25.3, 54.1, 120.6, 122.2, 126.2, 128.3, 128.6, 128.9, 135.8, 137.5, 141.3, 151.4, 160.0; *m/z* (EI, %) 607 (13) [M^+], 536 (4) [$M^+ - 2Cl$], 441 (28), 351 (4), 248 (2), 157 (6), 93 (100), 78 (14), 66 (34); HRMS: *m/z* calcd, 629.08146; found, 629.08081 [$C_{23}H_{23}N_3Cl_2PtNa^+$; $(M + Na)^+$].

Biological Studies. *Electrophoretic Mobility Shift Assay (EMSA).* Circular pBR322 plasmid DNA (1.5 μg, Thermo Scientific) was incubated with dilution series of cisplatin or complexes **2** and **3a−c** (5, 10, 25, 50 μM) in 1× TE buffer (10 mM Tris-HCl, 1 mM EDTA, pH 8.5) at 37 °C for 24 h (20 μL total sample volume). DNA samples without the addition of any test substance served as negative controls. Subsequent to the 24 h of incubation, samples were subjected to gel electrophoresis using 1% agarose gels in 0.5 TBE buffer (89 mM Tris, 89 mM boric acid, 25 mM EDTA, pH 8.3). Gels were stained with ethidium bromide, and DNA bands were visualized using UV excitation. Experiments were carried out at least in duplicate.

Ethidium Bromide Staining Assay. The extent of the Pt(II) complexes' DNA interaction was further assessed by a fluorescence-based ethidium bromide staining assay.[29,30] Salmon sperm DNA (SS DNA, Sigma-Aldrich) was pipetted into a black 96-well plate in 1× TE buffer to reach a final amount of 1 μg/100 μL assay volume and incubated with varying concentrations of cisplatin or complexes **3a−c** (5, 10, 25, or 50 μM, each concentration in triplicate) for 2 h at 37 °C. Afterward, 100 μL of a 10 μg/mL ethidium bromide solution in 1× TE buffer was added to each well. After 5 min of incubation, the fluorescence (λ_{ex} = 535 nm, λ_{em} = 595 nm) of each well was detected using a microplate reader (Tecan). Each fluorescence value was corrected by possible intrinsic compound and ethidium bromide background fluorescence (samples without DNA); the resulting values were then expressed as a percent of solvent controls (DMSO or DMF, 100% ethidium bromide binding = 100% fluorescence). Decreased fluorescence (%) is representative of impaired formation of ethidium bromide−DNA adducts due to DNA intercalation sites being blocked by the test compounds.

Quantitative Evaluation of Covalent Binding to Mammalian DNA in Cell-Free Medium. Solutions of double-helical CT DNA (42% G + C, mean molecular mass ca. 2×10^7) at a concentration of 0.32 mg mL^{-1} (1.0×10^{-3} M related to the phosphorus content) were incubated with compounds **3a**, **3b**, or **3c** (5×10^{-5} M) at a value of r_i = 0.05 in 0.1 mM NaCl at 37 °C. At regular intervals, aliquots of the reaction mixtures were withdrawn and exhaustively dialyzed first against 1 M NaCl (1 h, 4 °C) and then against ultrapure water. Subsequently, the samples were assayed by FAAS for platinum bound to DNA. DNA concentrations in the samples were verified by absorption spectrophotometry (ε_{260} = 6400 L mol^{-1} cm^{-1}).

Total Light Scattering. According to a literature procedure,[34] the experiments were carried out in cacodylate buffers (10 mM, pH 7.2), which, like the stock solutions of the test compounds in DMF, were filtered through 0.2 μm filters before use to avoid interference from dust particles. A solution of CT DNA (1.5 μM) was prepared in a 1 cm quartz cuvette in a total volume of 2.5 mL. Small volumes (1 μL) of compounds **3a**, **3b**, or **3c** were added to the CT DNA solution to obtain the desired

DOI: 10.1021/acs.jmedchem.5b00896
J. Med. Chem. 2015, 58, 6283−6292

concentration, and the solution was thoroughly mixed. The mixture was left undisturbed for 10 min at room temperature, and the total intensity light scattering was measured using a Varian Cary Eclipse spectrofluorophotometer with excitation and emission wavelengths set to 305 nm. The excitation and emission slit widths were 5 nm, and the integration time was set to 5 s. The scattered light was measured at a 90° angle relative to the incident beam.

Cell Cycle Analysis. 518A2 cells (5×10^4/mL) were grown on 6-well plates for 24 h and then treated with cisplatin or complexes **3a**−**c** for 24 h (cisplatin, 50 μM; **3a**, 30 μM; **3b**:, 5 μM; and **3c**, 500 nM). Solvent controls (DMSO or DMF) were treated identically. After fixation (70% EtOH, 4 °C), the cells were incubated with propidium iodide (PI, Roth) staining solution (50 μg/mL PI, 0.1% sodium citrate, 50 μg/mL RNase A in PBS) for 30 min at 37 °C. The fluorescence intensity of 10 000 single cells was measured at λ_{em} = 620 nm (λ_{ex} = 488 nm laser source) using a Beckman Coulter Cytomics FC 500 flow cytometer and analyzed (CXP Analysis, Beckman Coulter) for fractions of cells in G1, S, and G2/M phases. The percentage of apoptotic cells was assessed from sub-G1 peaks. The experiment for each sample was carried out in triplicate.

Chorioallantoic Membrane (CAM) Assay. Fertilized, specific pathogen-free (SPF) chicken eggs (VALO BioMedia) were bred in an incubator at 37 °C and a relative humidity of 60%. On day 5, windows (Ø 1.5−2 cm) were cut into the shell at the more rounded pole. The cavities were sealed with tape, and incubation was continued overnight. Rings of thin silicon foil (Ø 5 mm) were placed on the CAM with its developing blood vessels, and cisplatin or complexes **3a**−**c** (10 nmol in a volume of 10 μL of H_2O) were added. Solvent controls with respective amounts of DMSO or DMF were treated identically. The effects on the developing vasculature were documented after further incubation for 6 and 24 h using a light microscope (60× magnification, Traveler).[11,41,42] For each substance, the assay was performed at least in triplicate.

Ex Vivo Toxicity in Precision-Cut Kidney Slices..[43,44] Male Wistar rats (Charles River, Kissleg, Germany), 250−450 g, were housed under a 12 h dark/light cycle at constant humidity and temperature. Animals were permitted free access to tap water and standard lab chow. All experiments were approved by the Committee for Care and Use of Laboratory Animals of the University of Groningen and were performed according to strict governmental and international guidelines.

Fresh, viable rat kidneys were cut sagittally, and cylindrical cores of 7 mm diameter were prepared from the renal cortex with a manual tissue coring tool. Subsequently, PCKS with a wet weight of 5 mg were prepared in ice-cold Krebs−Henseleit buffer saturated with carbogen (95% O_2 and 5% CO_2) using a Krumdieck tissue slicer (Alabama R&D, Munford, AL, USA). The PCKS were preincubated at 37 °C for 1 h in Williams medium E supplemented with D-glucose monohydrate (275 mg/mL) and penicillin−streptomycin (100 U/mL and 100 μg/mL) and saturated with 80% O_2 and 20% CO_2 at pH 7.4. The slices were put in fresh medium, and incubation with cisplatin or complexes **3a**−**c** at different concentrations was continued for 24 h. Untreated kidney slices served as controls. The slices were transferred to 1 mL sonication solution (70% ethanol, 2 mM EDTA) in a safe-lock micro test tube containing glass MiniBeads, frozen in liquid nitrogen, and stored at −80 °C. Before analyzing the viability of the PCKS with the ATP bioluminescence assay kit CLS II (Roche), the samples were thawed and homogenized with a Mini-Beadbeater (Biospec Products) for 45 s. The ATP levels of the slices were normalized by means of protein concentrations determined by Lowry's method (Bio-Rad DC protein assay). The slices were dried overnight at 37 °C, 200 μL of 5 M NaOH was added, and incubation was continued at 37 °C for 30 min. The samples were diluted five times with Milli-Q water and homogenized with the Mini-Beadbeater for 40 s. The ATP content was corrected by the protein amount of each slice and expressed as pmol/μg protein. The protein content of the PCTS was determined by the Bio-Rad DC protein assay (Munich, Germany) using bovine serum albumin (BSA, Sigma-Aldrich, Steinheim, Germany) for the calibration curve. The viability of treated PCKS was expressed as a percent of the viability of controls set to 100%. For each test compound, at least two independent experiments were carried out in triplicate. Morphological changes induced in tissue sections by treatment with complexes **3a** or **3c** for 24 h were documented for three PCKS, which were incubated in 1 mL of buffered formalin at 4 °C overnight, followed by storage in 70% ethanol (4 °C). Dehydration of the PCKS, embedding in paraffin, sectioning, and staining with hematoxylin and eosin were carried out according to standard histological procedures.

■ ASSOCIATED CONTENT

Supporting Information

Instruments used; crystal structure determination and data of **3a**−**c**; cell lines and culture conditions; MTT assay; platinum accumulation (FAAS); partition coefficient; effect on bacterial morphology and on the induction of lysogenic bacteria; and histomorphology of PCKS treated with **3c**. The Supporting Information is available free of charge on the ACS Publications website at DOI: 10.1021/acs.jmedchem.5b00896.

■ AUTHOR INFORMATION

Corresponding Author

*E-mail: Rainer.Schobert@uni-bayreuth.de. Fax: +49 (0)921 552671. Phone: +49 (0)921 552679.

Notes

The authors declare no competing financial interest.

■ ACKNOWLEDGMENTS

We thank the COST Action CM1105 "Functional metal complexes that bind to biomolecules" for support and an STSM appropriation (J.K.M.). R.S. thanks the Deutsche Forschungsgemeinschaft for a grant (Scho 402/12-1), J.K. and V.B. thank the Czech Science Foundation for a grant (14-21053S), and J.K.M. thanks the Elite Study Program "Macromolecular Science", Elite Network of Bavaria, for its support.

■ ABBREVIATIONS USED

CAM, chorioallantoic membrane; EdtBr, ethidium bromide; EMSA, electrophoretic mobility shift assay; FAAS, flame atomic absorption spectrometry; MTT, 3-(4,5-dimethylthiazol-2-yl)-2,5-diphenyltetrazolium bromide; NHC, N-heterocyclic carbene; PCTS/PCKS, precission-cut tissue/kidney slices

■ REFERENCES

(1) Rosenberg, B.; VanCamp, L.; Trosko, J. E.; Mansour, V. H. Platinum compounds: a new class of potent antitumour agents. *Nature* **1969**, *222*, 385−386.

(2) Jamieson, E. R.; Lippard, S. J. Structure, Recognition, and processing of cisplatin-DNA adducts. *Chem. Rev.* **1999**, *99*, 2467−2498.

(3) Kartalou, M.; Essigmann, J. M. Mechanisms of resistance to cisplatin. *Mutat. Res., Fundam. Mol. Mech. Mutagen.* **2001**, *478*, 23−43.

(4) Wang, D.; Lippard, S. J. Cellular processing of platinum anticancer drugs. *Nat. Rev. Drug Discovery* **2005**, *4*, 307−320.

(5) Oh, G. S.; Kim, H. J.; Shen, A.; Lee, S. B.; Khadka, D.; Pandit, A.; So, H. S. Cisplatin-induced kidney dysfunction and perspectives on improving treatment strategies. *Electrolyte Blood Pressure* **2014**, *12*, 55−65.

(6) Dasari, S.; Tchounwou, P. B. Cisplatin in cancer therapy: molecular mechanisms of action. *Eur. J. Pharmacol.* **2014**, *740*, 364−378.

(7) Oehninger, L.; Rubbiani, R.; Ott, I. N-Heterocyclic carbene metal complexes in medicinal chemistry. *Dalton Trans.* **2013**, *42*, 3269−3284.

(8) Liu, W.; Gust, R. Metal N-heterocyclic carbene complexes as potential antitumor metallodrugs. *Chem. Soc. Rev.* **2013**, *42*, 755−773.

(9) Kaps, L.; Biersack, B.; Müller-Bunz, H.; Mahal, K.; Muenzner, J.; Tacke, M.; Mueller, T.; Schobert, R. Gold(I)-NHC complexes of antitumoral diarylimidazoles: structures, cellular uptake routes and anticancer activities. *J. Inorg. Biochem.* **2012**, *106*, 52−58.

(10) Muenzner, J.; Biersack, B.; Kaps, L.; Schobert, R.; Sasse, F. Synergistic "gold effects" of anti-vascular 4,5-diarylimidazol-2-ylidene

DOI: 10.1021/acs.jmedchem.5b00896
J. Med. Chem. 2015, 58, 6283−6292

gold(I) carbene complexes. *Int. J. Clin. Pharmacol. Ther.* **2013**, *51*, 44−46.
(11) Muenzner, J. K.; Biersack, B.; Kalie, H.; Andronache, I. C.; Kaps, L.; Schuppan, D.; Sasse, F.; Schobert, R. Gold(I) biscarbene complexes derived from vascular-disrupting combretastatin A-4 address different targets and show antimetastatic potential. *ChemMedChem* **2014**, *9*, 1195−1204.
(12) Mendes, F.; Groessl, M.; Nazarov, A. A.; Tsybin, Y. O.; Sava, G.; Santos, I.; Dyson, P. J.; Casini, A. Metal-based inhibition of poly(ADP-ribose) polymerase–the guardian angel of DNA. *J. Med. Chem.* **2011**, *54*, 2196−2206.
(13) Lease, N.; Vasilevski, V.; Carreira, M.; de Almeida, A.; Sanaú, M.; Hirva, P.; Casini, A.; Contel, M. Potential anticancer heterometallic Fe-Au and Fe-Pd agents: initial mechanistic insights. *J. Med. Chem.* **2013**, *56*, 5806−5818.
(14) Zhang, J.-J.; Che, C.-M.; Ott, I. Caffeine derived platinum(II) N-heterocyclic carbene complexes with multiple anti-cancer activities. *J. Organomet. Chem.* **2015**, *782*, 37−41.
(15) Zamora, A.; Pérez, S. A.; Rodríguez, V.; Janiak, C.; Yellol, G. S.; Ruiz, J. Dual antitumor and antiangiogenic activity of organoplatinum-(II) complexes. *J. Med. Chem.* **2015**, *58*, 1320−1336.
(16) Newman, C. P.; Deeth, R. J.; Clarkson, G. J.; Rourke, J. P. Synthesis of Mixed NHC/L Platinum(II) Complexes: Restricted rotation of the NHC group. *Organometallics* **2007**, *26*, 6225−6233.
(17) Patil, S.; Claffey, J.; Deally, A.; Hogan, M.; Gleeson, B.; Menéndez Méndez, L. M.; Müller-Bunz, H.; Paradisi, F.; Tacke, M. Synthesis, cytotoxicity and antibacterial studies of *p*-methoxybenzyl-substituted and benzyl-substituted N-heterocyclic carbene−silver complexes. *Eur. J. Inorg. Chem.* **2010**, *2010*, 1020−1031.
(18) Patil, S.; Deally, A.; Hackenberg, F.; Kaps, L.; Müller-Bunz, H.; Schobert, R.; Tacke, M. Novel benzyl- or 4-cyanobenzyl-substituted N-heterocyclic (bromo)(carbene)silver(I) and (carbene)(chloro)gold(I) complexes: synthesis and preliminary cytotoxicity studies. *Helv. Chim. Acta* **2011**, *94*, 1551−1562.
(19) Mosmann, T. Rapid colorimetric assay for cellular growth and survival: application to proliferation and cytotoxicity assays. *J. Immunol. Methods* **1983**, *65*, 55−63.
(20) Alvarez, M.; Robey, R.; Sandor, V.; Nishiyama, K.; Matsumoto, Y.; Paull, K.; Bates, S.; Fojo, T. Using the national cancer institute anticancer drug screen to assess the effect of MRP expression on drug sensitivity profiles. *Mol. Pharmacol.* **1998**, *54*, 802−814.
(21) Roundhill, E. A.; Burchill, S. A. Detection and characterisation of multi-drug resistance protein 1 (MRP-1) in human mitochondria. *Br. J. Cancer* **2012**, *106*, 1224−1233.
(22) Jong, N. N.; McKeage, M. J. Emerging roles of metal solute carriers in cancer mechanisms and treatment. *Biopharm. Drug Dispos.* **2014**, *35*, 450−462.
(23) Gupta, S.; Wulf, G.; Henjakovic, M.; Koepsell, H.; Burckhardt, G.; Hagos, Y. Human organic cation transporter 1 is expressed in lymphoma cells and increases susceptibility to irinotecan and paclitaxel. *J. Pharmacol. Exp. Ther.* **2012**, *341*, 16−23.
(24) Howell, S. B.; Safaei, R.; Larson, C. A.; Sailor, M. J. Copper transporters and the cellular pharmacology of the platinum-containing cancer drugs. *Mol. Pharmacol.* **2010**, *77*, 887−894.
(25) Zoldakova, M.; Kornyei, Z.; Brown, A.; Biersack, B.; Madarász, E.; Schobert, R. Effects of a combretastatin A4 analogous chalcone and its Pt-complex on cancer cells: a comparative study of uptake, cell cycle and damage to cellular compartments. *Biochem. Pharmacol.* **2010**, *80*, 1487−1496.
(26) Koepsell, H.; Lips, K.; Volk, C. Polyspecific organic cation transporters: structure, function, physiological roles, and biopharmaceutical implications. *Pharm. Res.* **2007**, *24*, 1227−1251.
(27) Cohen, G. L.; Bauer, W. R.; Barton, J. K.; Lippard, S. J. Binding of cis and trans dichlorodiammineplatinum(II) to DNA: evidence for unwinding and shortening of the double helix. *Science* **1979**, *203*, 1014−1016.
(28) Scovell, W. M.; Collart, F. Unwinding of supercoiled DNA by cis- and trans-diamminedichloroplatinum(II): influence of the torsional strain on DNA unwinding. *Nucleic Acids Res.* **1985**, *13*, 2881−2895.
(29) Spoerlein-Guettler, C.; Mahal, K.; Schobert, R.; Biersack, B. Ferrocene and (arene)ruthenium(II) complexes of the natural anticancer naphthoquinone plumbagin with enhanced efficacy against resistant cancer cells and a genuine mode of action. *J. Inorg. Biochem.* **2014**, *138*, 64−72.
(30) Di Salvo, A.; Dugois, P.; Tandeo, D.; Peltekian, M.; Kong Thoo Lin, P. Synthesis, cytotoxicity and DNA binding of oxoazabenzo[de]-anthracenes derivatives in colon cancer Caco-2 cells. *Eur. J. Med. Chem.* **2013**, *69*, 754−761.
(31) Sun, S.; Liu, W.; Cheng, N.; Zhang, B.; Cao, Z.; Yao, K.; Liang, D.; Zuo, A.; Guo, G.; Zhang, J. A thermoresponsive chitosan-NIPAAm/vinyl laurate copolymer vector for gene transfection. *Bioconjugate Chem.* **2005**, *16*, 972−980.
(32) Dong, X.; Wang, X.; He, Y.; Yu, Z.; Lin, M.; Zhang, C.; Wang, J.; Song, Y.; Zhang, Y.; Liu, Z.; Li, Y.; Guo, Z. Reversible DNA condensation induced by a tetranuclear nickel(II) complex. *Chem. - Eur. J.* **2010**, *16*, 14181−14189.
(33) Malina, J.; Farrell, N. P.; Brabec, V. DNA condensing effects and sequence selectivity of DNA binding of antitumor noncovalent polynuclear platinum complexes. *Inorg. Chem.* **2014**, *53*, 1662−1671.
(34) Vijayanathan, V.; Thomas, T.; Shirahata, A.; Thomas, T. J. DNA condensation by polyamines: a laser light scattering study of structural effects. *Biochemistry* **2001**, *40*, 13644−13651.
(35) Kankia, B. I.; Buckin, V.; Bloomfield, V. A. Hexamminecobalt-(III)-induced condensation of calf thymus DNA: circular dichroism and hydration measurements. *Nucleic Acids Res.* **2001**, *29*, 2795−2801.
(36) Rosenberg, B. Platinum complexes for the treatment of cancer. *Interdiscip. Sci. Rev.* **1978**, *3*, 134−147.
(37) Johnstone, T. C.; Alexander, S. M.; Lin, W.; Lippard, S. J. Effects of monofunctional platinum agents on bacterial growth: A retrospective study. *J. Am. Chem. Soc.* **2014**, *136*, 116−118.
(38) Reslova, S. The induction of lysogenic strains of Escherichia coli by cis-dichlorodiammineplatinum(II). *Chem.-Biol. Interact.* **1971**, *4*, 66−70.
(39) Sorenson, C. M.; Eastman, A. Mechanism of cis-diamminedichloroplatinum(II)-induced cytotoxicity: role of G2 arrest and DNA double-strand breaks. *Cancer Res.* **1988**, *48*, 4484−4488.
(40) Sorenson, C. M.; Eastman, A. Influence of cis-diamminedichloroplatinum(II) on DNA synthesis and cell cycle progression in excision repair proficient and deficient Chinese hamster ovary cells. *Cancer Res.* **1988**, *48*, 6703−6707.
(41) Norrby, K. In vivo models of angiogenesis. *J. Cell. Mol. Med.* **2006**, *10*, 588−612.
(42) Nitzsche, B.; Gloesenkamp, C.; Schrader, M.; Ocker, M.; Preissner, R.; Lein, M.; Zakrzewicz, A.; Hoffmann, B.; Höpfner, M. Novel compounds with antiangiogenic and antiproliferative potency for growth control of testicular germ cell tumours. *Br. J. Cancer* **2010**, *103*, 18−28.
(43) Parrish, A. R.; Gandolfi, A. J.; Brendel, K. Precision-cut tissue slices: applications in pharmacology and toxicology. *Life Sci.* **1995**, *57*, 1887−1901.
(44) de Graaf, I. A. M.; Olinga, P.; de Jager, M. H.; Merema, M. T.; de Kanter, R.; van de Kerkhof, E. G.; Groothuis, G. M. M. Preparation and incubation of precision-cut liver and intestinal slices for application in drug metabolism and toxicity studies. *Nat. Protoc.* **2010**, *5*, 1540−1551.
(45) Vickers, A. E.; Rose, K.; Fisher, R.; Saulnier, M.; Sahota, P.; Bentley, P. Kidney slices of human and rat to characterize cisplatin-induced injury on cellular pathways and morphology. *Toxicol. Pathol.* **2004**, *32*, 577−590.
(46) Bertrand, B.; Stefan, L.; Pirrotta, M.; Monchaud, D.; Bodio, E.; Richard, P.; Le Gendre, P.; Warmerdam, E.; de Jager, M. H.; Groothuis, G. M.; Picquet, M.; Casini, A. Caffeine-based gold(I) N-heterocyclic carbenes as possible anticancer agents: synthesis and biological properties. *Inorg. Chem.* **2014**, *53*, 2296−2303.
(47) Daum, S.; Chekhun, V. F.; Todor, I. N.; Lukianova, N. Y.; Shvets, Y. V.; Sellner, L.; Putzker, K.; Lewis, J.; Zenz, T.; de Graaf, I. A.; Groothuis, G. M.; Casini, A.; Zozulia, O.; Hampel, F.; Mokhir, A. Improved synthesis of N-benzylaminoferrocene-based prodrugs and

DOI: 10.1021/acs.jmedchem.5b00896
J. Med. Chem. 2015, 58, 6283−6292

evaluation of their toxicity and antileukemic activity. *J. Med. Chem.* **2015**, *58*, 2015−2024.

DOI: 10.1021/acs.jmedchem.5b00896
J. Med. Chem. 2015, 58, 6283−6292